Stability research of the cavity under the action of the drilling mechanism based on the inverse effect of cavity expansion method

Gaowei Xu[1], Yuebao Wang[1], Zhenjuan Tang[1], Huimin Fang[2], Junxiao Liu[3*], Yanxiang Chen[4*]

(1. *Department of Automotive Engineering, Shandong Jiaotong University, Jinan 250357, China*;
2. *School of Agricultural Engineering, Jiangsu University, Zhenjiang 212013, Jiangsu, China*;
3. *School of Mechanical and Electrical Engineering, Hainan University, Haikou 570228, China*;
4. *College of Civil and Environmental Engineering, Hunan University of Science and Engineering, Yongzhou 425199, Hunan, China*)

Abstract: Cavity maintenance is critical for ensuring the early growth and development of transplanted crops. A dense soil layer formed by a non-circular gear–parallel four-bar drilling mechanism serves as the key link between the drilling process and cavity stability. To optimize the operating parameters of the drilling mechanism for enhanced soil–machine interaction, this study systematically analyzed its structural configuration and working principles. Based on the inverse effect of cavity expansion theory, an elasto-plastic mechanical model of cavity surrounding soil is established, and the critical condition for cavity maintenance is derived. Using measured soil mechanical parameters at different moisture contents combined with the critical condition, the critical shear stress undertaken by the dense soil layer is calculated to determine the optimization objectives. Key response indicators and influencing factors are identified through the elasto-plastic model. A quadratic orthogonal rotary central composite design is adopted in soil-bin tests to establish regression equations between cavity maintenance indicators and influencing factors. Response surface methodology is employed to analyze effect trends and interaction effects, and a multi-objective optimization method based on the regression model is proposed to obtain the optimal parameter combination. Experimental results demonstrate that the optimized drilling parameters significantly improve cavity stability and operational performance. This study provides a theoretical basis and practical guidance for optimizing the operating parameters of drilling mechanisms from the perspective of soil mechanics.

Keywords: cavity transplanting, cavity drilling, model for the cavity maintenance, optimization
DOI: 10.25165/j.ijabe.20261903.10386

Citation: Xu G W, Wang Y B, Tang Z J, Fang H M, Liu J X, Chen Y X. Stability research of the cavity under the action of the drilling mechanism based on the inverse effect of cavity expansion method. Int J Agric & Biol Eng, 2026; 19(3): 50–60.

1 Introduction

Cavity transplanting technique is an agricultural practice primarily employed in hilly and mountainous regions, involving transplanting crop seedlings[1,2] into artificially constructed cavities. The core component of this technique involves the excavation and preparation of the cavity. Proper formation and maintenance of the cavity are critical factors that significantly influence the early growth and development of transplanted crops within the cavity transplanting system[3,4].

Currently, three types of cavity drilling device configurations have been developed for transplanting applications: manual drilling devices, multi-linkage drilling mechanisms[5-7], and intermittent drilling devices[8,9]. However, these conventional systems present several technical challenges: excessive labor requirements during operation, significant variation in cavity diameter, and limited operational reliability.

To address the aforementioned challenges, the authors have developed a non-circular gear-parallel four-bar drilling mechanism[10,11]. This design utilizes the variable-velocity characteristics of the parallel four-bar mechanism to approximate uniform linear motion, thereby compensating for the operating velocity of the mechanism. Under sustained implement operation, this configuration forms deep, high-precision transplanting cavities that meet the stringent requirements for crop transplantation in hilly and mountainous terrain. Under the rotational compression of the drilling device, a dense layer forms on the cavity surface, which prevents soil from migrating into the cavity interior due to the unloading effect of the drilling cavity and thus maintains the stability of the cavity.

The borehole unloading effect is a fundamental factor affecting cavity stability, and it is also an important factor leading to the complexity of the cavity maintenance mechanism[12]. Before drilling the cavity, the soil is in a state of initial relative equilibrium and stability. Borehole unloading disrupts the original stress balance of the soil, manifesting as relaxation of the soil adjacent to the cavity towards the cavity side[13]. This lateral deformation caused by unbalanced stress is the reason for the collapse of the drilled cavity. Therefore, the cylindrical cavity expansion theory can be used to describe the unloading process of the borehole, which can be regarded as the inverse process of cylindrical cavity expansion.

Vesic[14] provided the fundamental solutions for spherical and cylindrical expansion problems based on the Mohr-Coulomb

Received date: 2025-12-17 **Accepted date:** 2026-04-07
Biographies: Gaowei Xu, PhD, Associate Professor, research interest: agricultural machinery, Email: 202107@sdjtu.edu.cn; **Yuebao Wang**, ME candidate, research interest: agricultural machinery, Email: 25104030@stu.sdjtu.edu.cn; **Zhenjuan Tang**, ME, research interest: electromechanical control, Email: 202092@sdjtu.edu.cn; **Huimin Fang**, PhD, Associate Professor, research interest: agricultural equipment, Email: fanghuimin@ujs.edu.cn.
***Corresponding author: Junxiao Liu**, PhD, Associate Professor, research interest: agricultural machinery. School of Mechanical and Electrical Engineering, Hainan University, Haikou 570228, China. Email: 995229@hainanu.edu.cn; **Yanxiang Chen**, PhD, Senior Engineer, research interest: geotechnical mechanics. College of Civil and Environmental Engineering, Hunan University of Science and Engineering, Yongzhou 425199, Hunan, China. Email: chenyanxiang2377@huse.edu.cn

condition, which have been widely used in various fields of geotechnical engineering. Zhang et al.[15] proposed a calculation method for soil resistance around piles based on Vesic's circular hole expansion theory. Gharsallaoui et al.[16] calculated the ultimate bearing capacity at the tip of a pile embedded in rock masses based on the cavity expansion theory. Suman et al.[17] proposed cylindrical and spherical cavity expansion theories to evaluate the end bearing capacity of tapered piles by introducing a tapering factor. Chen et al.[18] proposed a calculation method for the bond strength between pressure grouting anchor bolts and soil interfaces based on the theory of viscoelastic-plastic circular hole expansion. Li et al.[19] proposed an analytical approach of large-strain cylindrical cavity expansion for analyzing the cylindrical compaction grouting problem considering pressure filtration. At present, the theory of circular hole expansion has been mainly applied to analyze the effects of pile and anchor embedded in the soil on the nearby soil forces, and the reverse process of the theory has not been applied to the stability analysis of drilling holes.

In conclusion, this paper applies the reverse process of cavity expansion to the stability research of mechanized drilling, considering the effect of borehole unloading. On this basis, an elastic-plastic mechanical critical theory model for the stability of cavity maintenance was established. Using the critical theory model, the key operating parameters of both the drilling mechanism and soil properties affecting stability were identified. By combining the model with soil mechanical parameters under different moisture contents, the critical shear stress borne by the dense soil layer on the cavity wall is also obtained, providing theoretical guidance for the optimization of the subsequent drilling mechanism's operating parameters. Building on this theoretical work, systematic experimental studies were conducted to examine the influence of each parameter on the shear stress of the dense soil layer, elucidating their respective impact patterns on cavity maintenance. Subsequently, an optimal combination of operating parameters was determined through a comprehensive analysis, in conjunction with the critical shear stress value of the compacted soil layer obtained from the critical theory model.

2 Materials and methods

2.1 Composition and operating principle of the drilling mechanism

The structural diagram of the drilling mechanism for the cavity is shown in Figure 1. It comprises two primary subsystems, a non-circular gear-parallel four-bar linkage and a drilling device.

The noncircular gear transmission system consists of gears (1 and 3), while the gear transmission mechanism includes spur gears (2, 4, and 5). Notably, spur gear 2 is coaxially fixed to non-circular gear (3), ensuring synchronized rotation. The parallel four-bar linkage is formed by double cranks (AB and CD), the frame (AC), and the connecting rod (BD), which operates in conjunction with the gear transmission system.

The drilling device (8) is vertically mounted on the connecting rod (BD). A flexible transmission shaft (6), coupled with a bevel gear set (7), transfers rotational motion from the drive system to the drilling device. Uniform rotary power is thus transmitted via shaft (6), enabling the controlled rotation of the drilling device (8).

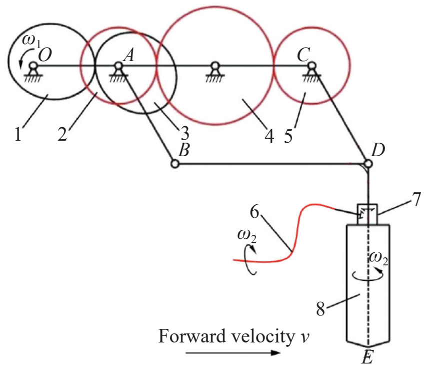

1. Non-circular gear; 2. Spur gear; 3. Non-circular gear; 4. Spur gear; 5. Spur gear; 6. Flexible transmission shaft; 7. Bevel gear set; 8. Drilling device. Note: v represents the operating velocity of the mechanism; *AB* represents the crank 1; *CD* represents the crank 2; *BD* represents the linkage; *OAC* represents the frame; ω_1 represents the rotational speed of crank 1; ω_2 represents the rotational speed of drilling device.

Figure 1 Structural diagram for the cavity drilling mechanism

The drilling process begins with uniform rotational motion transmitted through non-circular gear (1). This motion is converted into variable-speed rotation via the non-circular gear mechanism and subsequently output through non-circular gear (3). The modulated rotation is then transferred to cranks (AB and CD) via a spur gear transmission system, inducing variable-velocity oscillatory motion in connecting rod (BD).

To maintain consistent cavity diameter and compensate for the implement's forward velocity, the drilling device (8) is synchronized with the variable-speed oscillatory motion of the connecting rod (BD). This generates a horizontal velocity component that opposes the implement's advancement during soil interaction. Concurrently, the flexible transmission shaft (6)—driven by a constant-speed power source—imparts steady rotation to drilling device (8), enabling simultaneous oscillatory and rotary motion.

During the rotational extrusion process of drilling device (8), a dense soil layer forms along the inner wall of the cavity. This layer effectively mitigates soil displacement into the cavity induced by drilling-induced unloading, thereby ensuring structural stability. Through the combined mechanism, the variable-speed parallel four-bar linkage drilling system successfully achieved mechanized, continuous drilling operation of cavities with a depth of 20 cm. The drilling process of the drilling mechanism is shown in Figure 2.

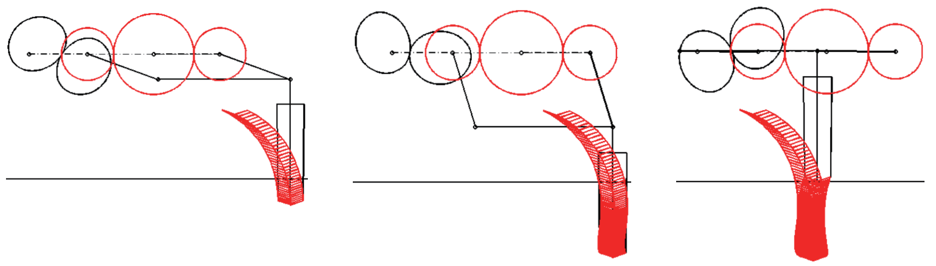

a. Drilling device begins to interact with the soil under the drilling mechanism b. Drilling device reaches the maximum drilling depth c. Drilling device retracts from the formed cavity

Figure 2 Drilling process of the drilling mechanism

A self-propelled platform integrated into the drilling mechanism, illustrated in Figure 3, consists of two main components: a parallel four-bar linkage drilling mechanism with non-circular gears and an extended-range electric rubber-tracked chassis.

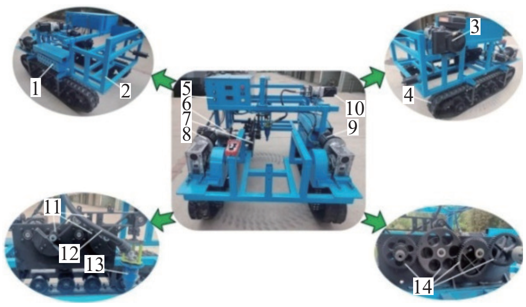

1. Power battery; 2. Frame of rubber tracked chassis; 3. Range extender; 4. Rubber-tracked chassis; 5. Electronic control module; 6. DC motor 6; 7. Drilling mechanism; 8. DC motor 8; 9. DC motor 9; 10. DC motor 10; 11. Parallel four-bar linkage; 12. Flexible shaft; 13. Drilling device; 14. Noncircular gear and spur gear transmission system

Figure 3 Structural diagram for the experimental platform

The system operates through coordinated electromechanical control, where the tracked chassis is propelled by two independently controlled DC (direct current) motors (8 and 9) with adjustable speed settings. The drilling mechanism is powered by DC motor (7), which drives the noncircular gear and spur gear transmission system (14) to actuate the four-bar linkage mechanism (11). Speed regulation for this subsystem is achieved via the upper knob on the electronic control module (5). Simultaneously, the drill bit (13) is rotated by DC motor (10) through a flexible shaft (12), with its rotational speed similarly controlled by the upper knob on the electronic control module (5). The self-propelled platform establishes a reliable foundation for subsequent soil-bin experiments of cavity drilling operation.

2.2 Research workflow for cavity maintenance

The research workflow is illustrated in Figure 4. Firstly, an elastic-plastic mechanical model for the dense soil layer surrounding the cavity was established based on the inverse effect of cavity expansion, from which the critical condition of the dense soil layer for cavity stability was derived. The corresponding critical shear stress borne by the dense soil layer was then estimated by applying soil parameters from direct shear and triaxial compression tests to the critical condition.

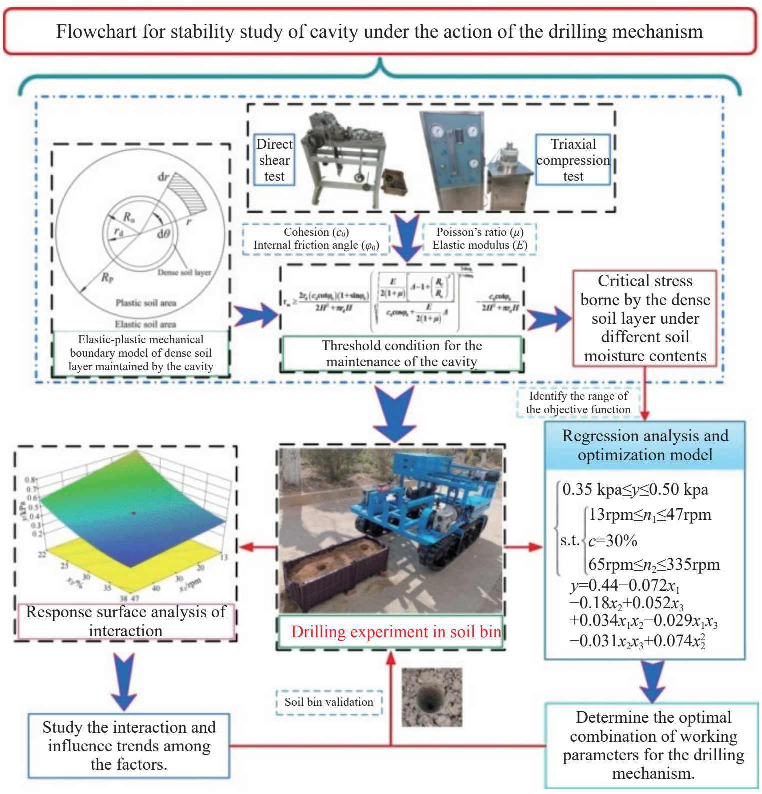

Figure 4 Flowchart for stability research of cavity under the action of the drilling mechanism

Secondly, a soil-bin drilling experiment was conducted to investigate the influence of the drilling mechanism's operating parameters on the shear stress within the dense soil layer. A regression equation was subsequently established to quantify this relationship. Furthermore, by integrating the previously determined critical shear stress borne by the dense soil layer of the cavity, an optimization objective was defined. Based on this, a parameter optimization model was constructed to determine the optimal set of operating parameters for the drilling mechanism.

Finally, a soil-bin drilling experiment was performed using the optimized operating parameters to validate the accuracy of the optimization model.

This research provides a transferable framework for studying the stability of cavity drilling across diverse soil types. The flowchart involves measuring the mechanical parameters of soil and integrating them with the established critical theory model to estimate the critical shear stress borne by the dense soil layer. This subsequently defines the range for the optimization objective. Drilling experiments can then be conducted to determine the optimal operating parameters of the drilling mechanism.

2.3 Establishment of the critical theory model for cavity maintenance

The soil mass was initially in a state of stable equilibrium under in-situ stress conditions. However, cavity drilling operations induced significant stress redistribution, primarily through lateral unloading[20]. This process disrupted the original stress field, leading to subsequent relaxation effects[21].

The lateral deformation caused by stress relaxation and time-dependent creep represents a significant factor in cavity collapse[18]. Therefore, the post-drilling unloading can be analytically modeled using cylindrical cavity expansion theory, which captures its inverse mechanical behavior[22–23].

2.3.1 Basic assumptions

The theoretical model is developed based on the following fundamental assumptions[24]:

1) The soil medium is idealized as a saturated, homogeneous, and isotropic material exhibiting elastic-perfectly plastic behavior.

2) The analysis considers small-strain cavity expansion within an infinite soil mass.

3) Soil shear strength in the plastic zone is governed by the Mohr-Coulomb failure criterion.

4) The far-field soil beyond the plastic zone is regarded as an isotropic linear elastic material.

2.3.2 Stress state analysis of the cavity

The cavity, formed through the interaction between the drilling mechanism and the surrounding soil, is equivalent to an ideal cylindrical cavity within an infinite soil mass (Figure 5).

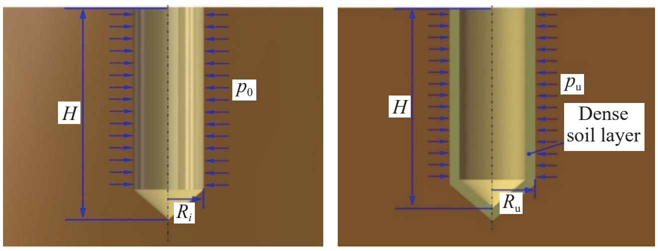

a. Cavity configuration assuming absence of dense soil layer

b. Cavity configuration with the dense soil layer

Figure 5 Stress redistribution analysis following cavity

Following the formation of the cavity, assuming no dense soil layer develops on the cavity wall, the initial radius of the cavity is denoted as r_i, with an equilibrium stress of p_0 (Figure 5a).

As the drilling device retracts from the cavity, an instantaneous pressure reduction occurs at the cavity wall. Given the surrounding soil's elastic state, this pressure drop induces a progressive contraction of the cavity under sustained earth pressure loading. The consequent stress redistribution disrupts the initial equilibrium condition, leading to time-dependent radial displacement development. As the cavity radius (R_i) decreases below a critical threshold, the soil at the cavity wall undergoes a transition from elastic to plastic state. Continuous reduction of the cavity radius (R_i) leads the system to reach a limiting plastic state, defined by a critical radius (R_u) and corresponding radial stress (p_u) that satisfies the Mohr-Coulomb failure criterion (Figure 4b).

Therefore, to ensure stress equilibrium within the cavity system, the load that the dense soil layer can bear should not be lower than p_u (Figure 5b). The analysis reveals that cavity drilling induces a progressive evolution of the surrounding soil from an elastic to a plastic state, ultimately forming a plastic zone around the cavity due to cavity unloading effects.

2.3.3 Stress equilibrium analysis

The mechanical analysis of the cavity problem was formulated under the plane strain assumption, where stress, deformation, and displacement components were considered as functions solely of the cross-sectional coordinates (x, y), with no variation along the axis perpendicular to the cross-section. Consequently, the cavity drilling problem can be solved as the inverse problem of axisymmetric circular cavity expansion.

Owing to the axial symmetry of the problem, all points lying on concentric circles experience identical stress states. Figure 6 presents the analysis of both elastic and plastic regions along with the corresponding stress states for the cavity system without a dense soil layer. At any given point, the principal stresses are characterized by the radial stress component (σ_r) and tangential stress component (σ_θ).

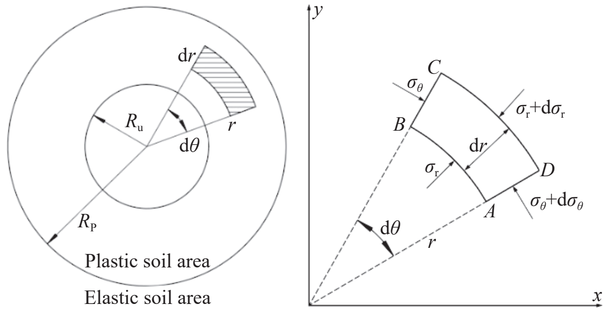

a. Elastic and plastic regions for the cavity

b. Mechanical analysis of plastic region for the cavity

Figure 6 Detailed analysis of both elastic and plastic regions along with the corresponding stress states for the cavity system

2.3.4 Theory model for the inverse effect of circular cavity expansion with the initial aperture

1) Fundamental equation

The mechanical analysis was performed on an arbitrary unit within the soil mass surrounding the circular cavity, yielding the following equilibrium differential equation[25]:

$$\frac{\partial \sigma_r}{\partial r} + \frac{\sigma_r - \sigma_\theta}{r} = 0 \tag{1}$$

where, σ_r denotes the radial stress of soil, kPa; σ_θ represents the tangential stress of soil, kPa; and r is the radial distance from the center of the circular cavity to an arbitrary unit, mm.

2) Elastic solution for the inverse effect of cavity expansion

The elastic soil domain of the cavity is characterized by the following conditions:

$$D_e = \{r|r \geq a, p < p_c\} \cup \left\{r|r \geq R_p, p \geq p_c\right\} \tag{2}$$

where, a is the hole radius during circular cavity contraction, mm; p is the internal pressure acting on the wall of cavity during the contraction of circular hole, kPa.

In terms of the boundary conditions: $r = a$, $\sigma_r = p$; $r = \infty$, $\sigma_r = 0$, the stress field and displacement field in the elastic region are obtained as follows:

$$\sigma_r = p\left(\frac{a}{r}\right)^2 \tag{3}$$

$$\sigma_\theta = -p\left(\frac{a}{r}\right)^2 \tag{4}$$

$$u_r = \frac{1+\mu}{E}\sigma_r r \tag{5}$$

where, μ denotes the Poisson's ratio of soil mass; and E is the elastic modulus of soil mass, MPa.

3) Elasto-plastic solution for the inverse effect of cavity expansion under Mohr-Coulomb law

Given the well-established accuracy of the Mohr-Coulomb criterion in modeling soil plasticity[26–28], this study employs it to analyze the elasto-plastic behavior during cavity expansion.

For Mohr-Coulomb materials, the yield criterion[29] is expressed as:

$$(\sigma_r-\sigma_\theta)=(\sigma_r+\sigma_\theta)\sin\varphi_0+2c_0\cos\varphi_0 \tag{6}$$

where, φ_0 is the internal friction angle, °; and c_0 is the cohesion of soil mass respectively, kPa.

The onset of yielding in the surrounding soil of cavity occurs when the pressure (p) acting on the cavity wall decreases to the critical pressure (p_c), with the cavity radius (r) reduced to a, under the initial stress field conditions. By substituting Equations (3) and (4) into Equation (6), the critical contraction pressure for yielding of the cavity wall is derived as follows:

$$p_c=c_0\cos\varphi_0 \tag{7}$$

The pressure on the wall demonstrates a continuous decrease during this stage. When the stress in the elastic zone exceeded the pressure on the wall (p), contraction of the plastic zone occurred in the direction of the cavity. Based on Equation (1) and the boundary conditions, $r=a$, $\sigma_r=p$.

The stress field in the plastic zone can be determined as follows:

$$\sigma_r=(p+c_0\cot\varphi_0)\left(\frac{a}{r}\right)^{\frac{2\sin\varphi_0}{1+\sin\varphi_0}}-c_0\cot\varphi_0 \tag{8}$$

$$\sigma_\theta=\frac{1-\sin\varphi_0}{1+\sin\varphi_0}\left[(p+c_0\cot\varphi_0)\left(\frac{a}{r}\right)^{\frac{2\sin\varphi_0}{1+\sin\varphi_0}}-c_0\cot\varphi_0\right]-\frac{2c_0\cot\varphi_0}{1+\sin\varphi_0} \tag{9}$$

As $r=R_p$, $\sigma_r=\sigma_p=p_c$. The radial displacement (u_p) at the elastic-plastic interface is derived from Equations (3) to (5):

$$u_p=\frac{1+\mu}{E}\sigma_p R_p=\frac{1+\mu}{E}p_c R_p \tag{10}$$

Substituting Equation (8) into the Expression (10), the radial displacement field in the plastic zone can be expressed as:

$$u_p=\frac{1+\mu}{E}R_p\left[(p+c_0\cot\varphi_0)\left(\frac{a}{R_p}\right)^{\frac{2\sin\varphi_0}{1+\sin\varphi_0}}-c_0\cot\varphi_0\right] \tag{11}$$

Assuming the total volumetric strain induced by cavity shrinkage equals the sum of the volumetric changes in both elastic and plastic zones, this leads to the governing equation:

$$\pi\left(R_0^2-R_u^2\right)=\pi R_p^2-\pi\left(R_p-u_p\right)^2+\pi\left(R_p^2-R_u^2\right)\Delta \tag{12}$$

where, Δ is the average volume of plastic zone, mm³.

Expanding Equation (12) and neglecting the higher-order term of u_p^2, the equation can be simplified as:

$$\Delta-1+\left(\frac{R_0}{R_u}\right)^2=\left(\frac{R_p}{R_u}\right)^2\Delta+2u_p\frac{R_p}{R_u^2} \tag{13}$$

Substituting Equation (11) into Equation (12) yields:

$$\Delta-1+\left(\frac{R_0}{R_u}\right)^2=\frac{2(\mu+1)}{E}\left(\frac{R_p}{R_u}\right)^2\left[(p+c_0\cos\varphi_0)\left(\frac{R_u}{R_p}\right)^{\frac{2\sin\varphi_0}{1+\sin\varphi_0}}-c_0\cot\varphi_0\right]+\left(\frac{R_p}{R_u}\right)^2\Delta \tag{14}$$

In terms of the Equation (4), when $r=r_p$, $\sigma_r=-\sigma_\theta$, substituting this result into Equation (6) yields:

$$\sigma_p=c_0\cos\varphi_0 \tag{15}$$

Substituting Equation (15) into Equation (8) yields:

$$c_0\cos\varphi_0=(p+c_0\cot\varphi_0)\left(\frac{a}{r}\right)^{\frac{2\sin\varphi_0}{1+\sin\varphi_0}}-c_0\cot\varphi_0 \tag{16}$$

By further substituting Equation (16) into Equation (14), then the following equation is obtained:

$$\Delta-1+\left(\frac{R_0}{R_u}\right)^2=\left(\frac{R_p}{R_u}\right)^2\Delta+2\left(\frac{R_p}{R_u}\right)^2\frac{1+\mu}{E}(c_0\cos\varphi_0) \tag{17}$$

The radius of the plastic zone R_p can be determined from Equation (17):

$$R_p=R_u\sqrt{\frac{\frac{E}{2(1+\mu)}\left[\Delta-1+\left(\frac{R_0}{R_u}\right)^2\right]}{c_0\cos\varphi_0+\frac{E}{2(1+\mu)}\Delta}} \tag{18}$$

When $r=R_p$, by substituting Equation (18) into Equation (16), the governing equation can be derived for p_u:

$$p_u=c_0(\cos\varphi_0+\cot\varphi_0)\left(\sqrt{\frac{\frac{E}{2(1+\mu)}\left[\Delta+1-\left(\frac{R_0}{R_u}\right)^2\right]}{c_0\cos\varphi_0+\frac{E}{2(1+\mu)}\Delta}}\right)^{\frac{2\sin\varphi_0}{1+\sin\varphi_0}}-c_0\cot\varphi_0 \tag{19}$$

4) Critical theory model for cavity maintenance

After construction of a cavity, the lateral pressure acting on the plastic soil area gradually decreases[30]. To enhance structural stability, a dense soil layer was formed along the wall surface by the drilling mechanism through rotation of the drilling device. This layer withstands soil pressure under plastic failure conditions, as shown in Figure 7.

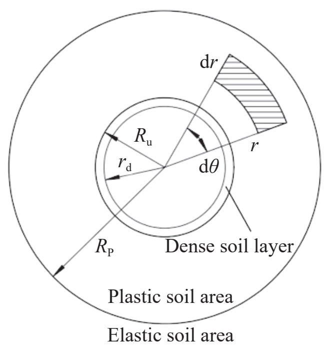

Figure 7 Mechanical structural analysis of dense soil layer adjacent to cavity

The present study focuses on conducting mechanical analysis of the differential element in the dense soil layer, where the analytical approach is detailed in Figure 8.

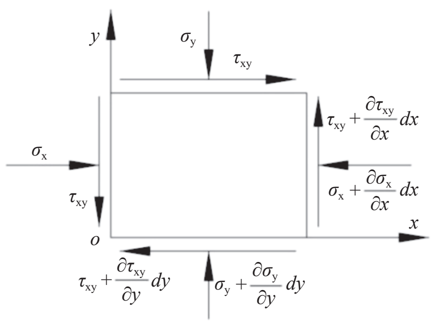

Figure 8 Stress analysis of differential soil element in the dense soil layer for the cavity

When the stress state of a differential element in the dense soil layer surrounding the cavity satisfies the yield criterion, the governing equation can be derived as follows:

$$\left(\sigma_x-\sigma_y\right)^2+\tau_{xy}^2=4\tau_m^2 \tag{20}$$

where, τ_m is the shear stress of the dense soil layer for the cavity, kPa; σ_x is the normal stress of dense soil layer received in x direction, kPa; σ_y is the normal stress of dense soil layer received in y direction, kPa.

By coupling the depth-dependent horizontal stress field (σ_x) with the cavity depth (H), the integrated horizontal force exerted by the dense soil layer on the plastic soil region is expressed as:

$$p_m=\int_0^H\sigma_x\mathrm{d}y=\frac{\tau_m H^2}{2r_d}+\frac{\pi\tau_m H}{2} \tag{21}$$

where, H is the depth of the cavity, mm; p_m is the stress of the drill-formed dense soil layer, kPa.

To prevent cavity collapse induced by reverse cavity effects, the stress (p_m) of the drill-formed dense soil layer must exceed the stress (p_u) in the surrounding plastic zone. Therefore, this requirement establishes the following relationship:

$$\tau_m\geq\frac{2r_d(c_0\cot\varphi_0)(1+\sin\varphi_0)}{2H^2+\pi r_d H}\cdot\left(\sqrt{\frac{\frac{E}{2(1+\mu)}\left[\Delta-1+\left(\frac{R_0}{R_u}\right)^2\right]}{c_0\cos\varphi_0+\frac{E}{2(1+\mu)}\Delta}}\right)^{\frac{2\sin\varphi_0}{1+\sin\varphi_0}}-\frac{c_0\cot\varphi_0}{2H^2+\pi r_d H} \tag{22}$$

Equation (22) indicates that the shear stress τ_m of the drill-formed dense soil layer depends on the parameters: cavity depth (H), cavity radius (r_d), internal friction angle (φ_0), cohesion (c_0), Poisson's ratio (μ), and modulus of elasticity (E) of the in-situ soil.

2.3.5 Case study analysis

In this section, a ZJ type strain-controlled direct shear apparatus (Nanjing Soil Instrument Factory Co., Ltd., Nanjing, Jiangsu, China) was used to obtain data on soil cohesion (c_0) and internal friction angle (φ_0). An HDSZ-30A triaxial testing machine (Nanjing Huade Soil Instrument Manufacturing Co., Ltd., Nanjing, China) was utilized to gather data on Poisson's ratio (μ) and elastic modulus (E). The tests were conducted on sandy loam soil samples from a drilling and planting site in Jinan region, Shandong Province, with moisture contents ranging from 20% to 40%. The experimental equipment is as shown in Figure 9.

a. ZJ-type direct shear apparatus   b. HDSZ-30A-type triaxial testing machine

Figure 9 Experimental equipment of soil cohesion and internal friction angle

Utilizing these parameters in conjunction with the predefined cavity dimensions (75 mm diameter and 180 mm height), the critical shear stress borne by the dense soil layer was calculated via Equation (22), as listed in Table 1.

Figures 10 and 11 illustrate the variation trends in the critical shear stress (τ_m) borne by the dense soil layer and the in-situ soil cohesion (c_0) across a soil moisture content (w) range of 20% to 40%. Figure 10 reveals a rapid decline in the critical shear stress (τ_m) borne by the dense soil layer with increasing soil moisture content. This value plummets from 0.71 to 0.53 kPa, accompanied by an increase in moisture content from 20% to 24%. As the soil moisture content rises further from 24% to 30%, the critical shear stress continues to decline, dropping from 0.53 to 0.37 kPa. Notably, the rate of this decrease is significantly slower than that seen during the increase from 20% to 24%. As the soil moisture content is raised successively from 30% to 36% and then to 40%, the critical shear stress shows a successive reduction from 0.37 to 0.29 kPa and finally to 0.23 kPa, at a progressively slower rate of decrease. The data from Figures 10 and 11 collectively reveal that the variation trends of the critical shear stress (τ_m) borne by the dense soil layer and the cohesion (c_0) for the in-situ soil exhibit a strong correspondence over the soil moisture content range of 20% to 40%.

Table 1 Mechanical parameters of sandy loam soil and estimated critical shear stress for the dense soil layer under varying moisture contents

Soil moisture content w/%	Cohesion c_0/kPa	Internal friction angle φ_0/(°)	Poisson's ratio μ	Modulus of elasticity E/MPa	Critical shear stress τ_m/kPa
20	34.5	21.1	0.37	30.12	0.71
24	29.8	18.6	0.39	25.67	0.53
30	21.5	16.2	0.41	17.85	0.37
36	16.9	13.2	0.43	10.18	0.29
40	13.8	12.1	0.44	6.96	0.23

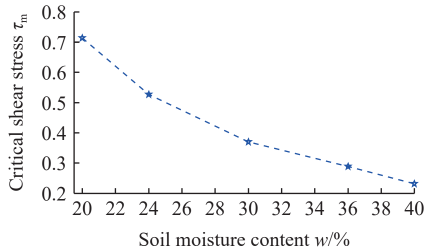

Figure 10 Variation trend in the critical shear stress borne by the dense soil layer across a soil moisture content range of 20% to 40%

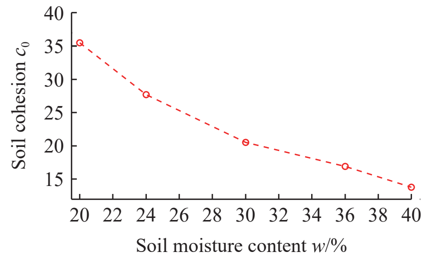

Figure 11 Variation trend in the in-situ soil cohesion across a soil moisture content range of 20% to 40%

The observed behavior patterns can be attributed to the following underlying mechanisms: (1) The stability of an in-situ soil mass is fundamentally governed by its cohesion. During drilling, this inherent equilibrium is disrupted, leading to inward migration of soil particles near the borehole under cohesive forces. When such displacement exceeds a critical threshold, the drilled cavity collapses. Therefore, the variation in critical shear stress (τ_m) borne by the dense soil layer not only reflects changes in soil cohesion but also validates the accuracy of the critical theory model used for cavity maintenance. (2) As the soil moisture content increases from 20% to 40%, the soil transitions from an unsaturated to a nearly saturated state. This elevation in moisture content raises the proportion of free water, leading to the gradual disappearance of menisci and a corresponding decrease in capillary pressure. The increased free water weakens inter-particle attraction, as reflected by a reduction in matrix suction, which in turn diminishes the cohesion of the in-situ soil. Meanwhile, the rise in soil moisture content leads to a continuous increase in saturation degree, progressively approaching full saturation. Correspondingly, capillary water pressure declines to its minimum, accompanied by a persistent decrease in soil cohesion at a progressively slowing rate.

2.4 Experimental study on the cavity drilling of drilling mechanism

2.4.1 Determination of experimental factors and indicators

For the drill-formed cavity with given depth (H) and radius (r), the theoretical model identified the critical stability parameters: internal friction angle (φ_0) and cohesion (c_0) of the soil matrix. As demonstrated in the literature[31], φ_0 and c_0 are controlled by moisture content (w) and bulk density (ρ_b). The shear stress (τ_m) of dense soil layer serves as the primary stability metric.

The quality of cavity drilling is governed by the dynamic interaction between the drilling system and the soil formation. Based on the established theoretical model and operational parameters of the drilling system, three critical factors influencing the maintenance of cavity have been identified: operating frequency of the drilling mechanism, moisture content of in-situ soil, and rotational speed of the drilling device.

The structural stability of the cavity primarily depends on the soil-drilling mechanism interactions. Field observations revealed that the shallow subsurface zone (0-5 cm in depth) shows significantly higher susceptibility to cavity collapse. Therefore, the shear stress of the mechanically dense soil layer along the cavity wall within this critical zone serves as a key parameter for structural stability assessment.

2.4.2 Experimental contents and methods

Based on preliminary single-factor experiments, literature review[31-32], and experimental indices, the operational parameters for the drilling mechanism were determined: operating frequency range of 13-47 r/min, soil moisture content range of 20%-40%, and rotational speed range of 65-335 r/min for the drilling device. Each factor was evaluated at five distinct levels to ensure comprehensive analysis. Subsequently, soil-bin experiments were conducted to study cavity excavation by the drilling mechanism. A quadratic orthogonal rotation central composite design was employed to determine the optimal parameter combinations for both soil conditions and drilling device operation. Experimental factors and levels are summarized in Table 2.

Table 2 Experimental variables & codes

Codes	Factors		
	x_1	x_2	x_3
	Operating frequency of the drilling mechanism/r·min^{-1}	Soil moisture content/%	Rotational speed of the drilling device/r·min^{-1}
1.682	47	40±1	335
1	40	36±1	280
0	30	30±1	200
–1	20	24±1	120
–1.682	13	20±1	65

The soil moisture content was measured using a JK-100F hygrometer (accuracy: ±0.5%) (Tianjin Huayin Construction Engineering Instrument Technology Co., Ltd., Tianjin, China). The shear stress (τ_m) of the dense soil layer was determined using a WXSZB-2.0 miniature vane shear apparatus (Xinghua Youke Instrumentation Co., Ltd., Xinghua, Jiangsu, China) to measure the average value obtained by taking several points uniformly within the 0-5 cm depth interval post-drilling in situ. The experimental configuration and instrumentation are shown schematically in Figure 12.

a. Drilling experiment of soil-bin

b. WXSZB-2.0 miniature vane shear apparatus

c. JK100F moisture content meter

Figure 12 Experimental configuration and instrumentation

3 Results and analysis

3.1 Experimental result and analysis

The experimental design and results are summarized in Table 3. The analysis of variance (ANOVA) for each response variable is listed in Table 4, with x_1, x_2, and x_3 representing the coded levels of the independent variables.

Table 3 Experimental design and results

No.	Factors			Indices
	x_1	x_2	x_3	y/kPa
1	–1 (20)	–1 (24)	–1 (120)	1.07
2	1 (40)	–1 (24)	–1 (120)	0.94
3	–1 (20)	1 (36)	–1 (120)	0.78
4	1 (40)	1 (36)	–1 (120)	0.71
5	–1 (20)	–1 (24)	1 (280)	1.33
6	1 (40)	–1 (24)	1 (280)	1.01
7	–1 (20)	1 (36)	1 (280)	0.84
8	1 (40)	1 (36)	1 (280)	0.73
9	–1.628 (13)	0 (30)	0 (200)	0.95
10	1.628 (47)	0 (30)	0 (200)	0.74
11	0 (30)	–1.628 (20)	0 (200)	1.36
12	0 (30)	1.628 (40)	0 (200)	0.69
13	0 (30)	0 (30)	–1.628 (65)	0.68
14	0 (30)	0 (30)	1.628 (335)	0.86
15	0 (30)	0 (30)	0 (200)	0.83
16	0 (30)	0 (30)	0 (200)	0.83
17	0 (30)	0 (30)	0 (200)	0.85
18	0 (30)	0 (30)	0 (200)	0.84
19	0 (30)	0 (30)	0 (200)	0.84
20	0 (30)	0 (30)	0 (200)	0.85
21	0 (30)	0 (30)	0 (200)	0.84
22	0 (30)	0 (30)	0 (200)	0.84
23	0 (30)	0 (30)	0 (200)	0.85

Statistical analysis was performed using Design-Expert 8.0 software. A reduced quadratic model was developed by removing non-significant terms (p>0.05), resulting in the final regression equation that relates the response variables to the coded independent factors:

$$y = 0.44 - 0.072x_1 - 0.18x_2 + 0.052x_3 + 0.034x_1x_2 - 0.029x_1x_3 - 0.031x_2x_3 + 0.074x_2^2 \quad (23)$$

The influence of independent variables on response parameters was evaluated through response surface methodology using Design-Expert 8.0 software, with the resulting surface plots illustrated in Figure 13.

Figure 13a illustrates the effects of soil moisture content and rotational speed of the drilling device on the shear stress of the dense soil layer, while other factors are maintained at the threshold level. Under the constant operating frequency of the drilling mechanism, the shear stress of the dense soil layer exhibits a negative correlation with increasing soil moisture content. This phenomenon is attributed to the progressive saturation of the dense soil layer as the moisture content increased. The saturation process diminishes capillary suction between soil particles, consequently reducing inter-particle cohesion. This reduction in cohesive forces ultimately leads to decreased shear stress in the dense soil layer of the cavity.

Table 4 Variance analysis of regression model

Experiment indicators	Sources of variation	Sum of squares	Freedom	F	p
y	Model	0.65	7	65.99	<0.0001**
	x_1	0.071	1	50.56	<0.0001**
	x_2	0.43	1	305.54	<0.0001**
	x_3	0.037	1	26.57	<0.0001**
	x_1x_2	9.113×10^{-3}	1	6.51	0.0221*
	x_1x_3	6.613×10^{-3}	1	4.72	0.0462*
	x_2x_3	7.813×10^{-3}	1	5.58	0.0321*
	x_2^2	0.087	1	62.42	<0.0001**
	Residual	0.021	15		
	Sum	0.67	22		

Note: **extremely significant (p<0.01); *significant (0.01≤p≤0.05).

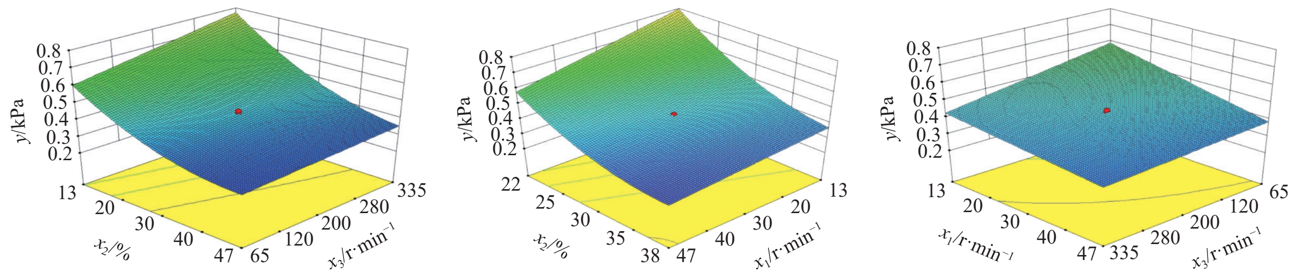

a. Influence of soil moisture content and rotational speed of the drilling device on the shear stress of the soil compact layer at the zero level of other factors

b. Influence of operating frequency of the drilling mechanism and soil moisture content on the shear stress of the dense soil layer at the zero level of other factors

c. Influence of soil moisture content and rotational speed of the drilling device on the shear stress of the dense soil layer at the zero level of other factors

Figure 13 Response surface of factor to experiment index

When both the soil moisture content and the rotational speed of the drilling device are below the threshold level, the shear stress of the dense soil layer significantly increases with the rotational speed. Although the soil compaction effect is relatively weak under below-threshold rotational speeds, a prolonged interaction between the drilling device and soil particles persists during both the penetration and subsequent extraction phases. As the rotational speed of the drilling device continues to increase, its compaction effect on the soil becomes significantly more pronounced. Therefore, under these conditions, the shear stress of the dense soil layer exhibits a positive correlation with the rotational speed of the drilling device. These results suggest that even under conditions typically considered unfavorable for compaction, the dynamic interaction under below-threshold conditions could induce significant improvements in shear strength.

When the rotational speed exceeds the threshold level, the shear stress of the dense soil layer shows a small increase with the rotational speed. The reason is that the higher rotational speed imparts substantial kinetic energy to the soil particles during penetration, which causes cavity enlargement beyond the diameter of the drilling device. Due to an annular gap developing between the drilling device and the dense soil layer, the drilling device inhibits further densification of the surrounding soil matrix during retraction. Although the rotational speed of the drilling device increased, the total contact duration between the drilling device and cavity wall remained unchanged.

When the soil moisture content exceeds the threshold level, the shear stress of the dense soil layer shows a modest but consistent increase with the higher rotational speeds of the drilling device. This results in the water-saturated state of void spaces in the soil matrix. While higher rotational speed enhances soil compaction, this saturated condition limited further improvement in capillary cohesion between particles. Thus, this limitation prevents the significant shear stress enhancement in the dense soil layer within the cavity.

Figure 13b illustrates the relationship between the soil moisture content and the operating frequency of drilling mechanism on the shear stress of the dense soil layer, while other factors are maintained at the threshold level. When the operating frequency remains constant, the shear stress of the dense soil layer in the cavity exhibits an inverse correlation with the increasing soil moisture content. This results from progressive water saturation in soil voids, which weakens inter-particle cohesive bonds through reduced capillary cohesion. Ultimately, this mechanistic chain decreases shear stress in the dense soil layer.

Under the constant soil moisture conditions, the shear stress at the dense soil layer decreases with the increasing operating frequency of the drilling mechanism. This is attributed to reduced effective compaction duration at higher operating frequencies, resulting in insufficient particle rearrangement and consequent shear strength reduction.

Figure 13c illustrates the effects of drilling device rotational speed and operating frequency on the shear stress of the dense soil layer, while other factors are maintained at the threshold level.

Under the constant soil moisture content, when the operating frequency of the drilling mechanism exceeds the threshold level, the shear stress of the dense soil layer increases marginally with the rotational speed of the drilling device. In contrast to the former scenario, when the operating frequency remains below the threshold level, the shear stress exhibits a more pronounced increase with the rotational speed.

This phenomenon is attributed to the limited interaction between the drilling device and soil at higher operating frequencies. Under this condition, although the rotational speed increased, its impact on the shear stress of the dense soil layer remained essentially constant.

3.2 Parameters optimization

In the Jinan region of Shandong Province, the optimal soil moisture content for drilling planting operations is approximately 30%[33]. This section identifies the lower limit of the optimization objective (τ_t), by integrating the critical shear stress value of the dense soil layer (τ_m) corresponding to 30% of soil moisture content (as listed in Table 1) with the following analytical equation:

$$\tau_t \geq \lambda \tau_m \tag{24}$$

where, τ_t is the optimization objective for shear stress of the dense soil layer, kPa; and λ is the safety factor. The value range of safety factor λ is 1.5-2.0[34]. At this point, the value of λ is 1.7.

The upper limit for the optimization objective (τ_t) is set at approximately 0.65 kPa, with consideration given to the required maintenance duration, and the specific growth characteristics of the transplanted crops[35-36]. Consequently, the feasible range for τ_t is defined as:

$$0.65\ \text{kPa} \leq \tau_t \leq 0.80\ \text{kPa}$$

To determine the optimal experimental factor combination, an optimization model was developed with: experimental factor ranges as constraints, the shear stress of the dense soil layer in the wall of the cavity constrained to 0.65-0.80 kPa, and the regression equation from the experiment design as the objective function. The model equation is as follows:

$$\begin{cases} 0.65\ \text{kPa} \leq y \leq 0.80\ \text{kPa} \\ \text{s.t.} \begin{cases} 13\ \text{r/min} \leq n_1 \leq 47\ \text{r/min} \\ c = 30\% \\ 65\ \text{r/min} \leq n_2 \leq 335\ \text{r/min} \end{cases} \end{cases} \tag{25}$$

Multi-objective parameter optimization was performed using Design Expert 8.0 software. Based on the operational vibration requirements of the drilling mechanism[10], soil moisture conditions[37-39], and device reliability[40-42], an optimal parameter combination was identified as: a mechanism operating frequency of 34.9 r/min, soil moisture content of 30%, and rotational speed of 173.6 r/min for the drilling device. Regression Equation (23) with these parameters yielded a dense soil layer of the cavity with a shear stress of 0.78 kPa.

3.3 Experimental verification and analysis

To validate the accuracy of the parameter optimization model and the optimal operating combination of the drilling mechanism, a soil-bin verification experiment was conducted using the determined optimal parameter combination. The self-propelled platform (Figure 2) integrated into the drilling mechanism was specifically developed for the soil-bin experiment. Repeated cavity drilling experiments were performed under controlled conditions with the drilling mechanism operating at (35±0.5) r/min, soil moisture content maintained at (30±1)%, and the drilling device rotating at (174±3) r/min.

The shear stress of the dense soil layer was measured using a micro vane shear apparatus for five cavity sample groups, and the results are presented in Table 5. Experimental results demonstrated excellent agreement with the theoretical predictions. The measured average values included a rotational frequency of 34.7 r/min, a soil moisture content of 30.1%, and a drilling device rotational speed of 173.2 r/min. These parameters resulted in an average shear stress of 0.72 kPa within the dense soil layer (0-5 cm depth) of the cavity.

Table 5 Shear stress of the dense soil layer of five cavity sample groups

No.	Operating frequency of drilling mechanism/ $\text{r}\cdot\text{min}^{-1}$	Soil moisture content/%	Rotational speed of the drilling device/ $\text{r}\cdot\text{min}^{-1}$	Shear stress of 0-5 cm dense soil layer adjacent to the cavity wall/kPa
1	34.5	30.2	174	0.73
2	34.6	30.9	173	0.72
3	34.6	29.8	171	0.72
4	35.3	30.7	176	0.71
5	34.7	29.1	172	0.70
Average value	34.7	30.1	173.2	0.72

The relative errors between experimental measured and model-predicted values from five cavity sample groups are shown in Table 6. The maximum value of relative errors between the experimental measured and model-predicted values was 10.3%, and the minimum value was 6.4%. The observed discrepancies are attributed to two primary factors: the manual control of soil moisture content in the soil-bin, and the inherent shear stress distribution within the dense soil layer, which decreases progressively from the bottom to the top. This stress gradient results in the lowest shear stress occurring at the 0-5 cm depth, making this zone the most prone to cavity collapse and producing values that are lower than those predicted by the optimization model.

Table 6 Relative errors between experiment measured and model-predicted values of five cavity sample groups

Shear stress of the 0-5 cm dense soil layer adjacent to the cavity wall	1	2	3	4	5	Average value
Measured value/kPa	0.73	0.72	0.72	0.71	0.70	0.72
Theoretical value/kPa			0.78			
Relative error/%	6.4	7.7	7.7	8.9	10.3	8.2

To assess the differential effects, the comparative results for the cavities formed by treatment pairs 9-10, 11-12, and 13-14 in the experimental design (Table 3) are presented in Figure 14. To determine the strength of the interaction between soil and drilling device, blue pigment was incorporated into the drilling experiments[43-44]. A darker coloration indicates a more pronounced interaction between the drilling device and the soil.

The cavity formed under the lower operating frequency of 13 r/min (Figure 14a) demonstrates higher quality and roundness compared to that formed at 47 r/min (Figure 14b), under otherwise identical conditions (20% soil moisture, 200 r/min rotational speed of the drilling device). The superior outcome at 13 r/min is due to prolonged soil-contact time, which facilitates effective drilling. In contrast, the inferior cavity quality at 47 r/min is likely caused by the shorter soil-contact time and increased operational vibration associated with the higher rotation speed.

The cavity formed at the lower soil moisture of 20% (Figure 14c) demonstrates a harder texture of dense soil layer compared to that formed at 40% (Figure 14d), under otherwise identical conditions (30 r/min operating frequency, 200 r/min rotational speed of the drilling device). The superior mechanical properties at 20% soil moisture content are due to stronger inter-particle cohesion and higher shear strength. In contrast, the softer texture at 40% moisture is caused by the moisture-induced reduction in soil cohesion and shear strength, resulting from the enhanced lubricating effect of the increased water film between soil particles. This textural transition directly corroborates the results identified in experimental design 11 and 12.

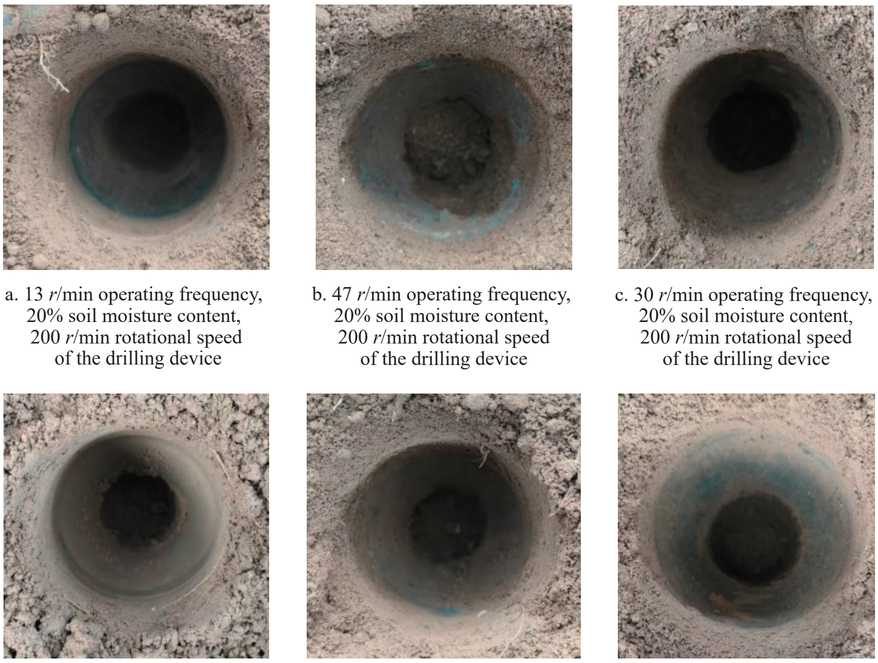

a. 13 *r*/min operating frequency, 20% soil moisture content, 200 *r*/min rotational speed of the drilling device

b. 47 *r*/min operating frequency, 20% soil moisture content, 200 *r*/min rotational speed of the drilling device

c. 30 *r*/min operating frequency, 20% soil moisture content, 200 *r*/min rotational speed of the drilling device

d. 30 *r*/min operating frequency, 40% soil moisture content, 200 *r*/min rotational speed of the drilling device

e. 30 *r*/min operating frequency, 30% soil moisture content, 65 *r*/min rotational speed of the drilling device

f. 30 *r*/min operating frequency, 30% soil moisture content, 335 *r*/min rotational speed of the drilling device

Figure 14 Comparative results for the cavities under a specified set of conditions

The cavity formed at the lower drilling device's rotational speed of 65 r/min (Figure 14e) exhibits a smaller diameter compared to that generated at 335 r/min (Figure 14f), under otherwise identical conditions (30 r/min operating frequency, 30% soil moisture content). The limited diameter at 65 r/min is attributed to the lower kinetic energy imparted to soil particles. Conversely, the enlarged cavity diameter at 335 r/min is caused by the higher rotational speed, which provides greater kinetic energy and imparts larger inertial forces to the soil particles, enabling them to be displaced beyond the physical confines of the drilling device.

4 Conclusions

This study establishes a comprehensive framework for analyzing and optimizing cavity stability in drilling mechanisms. The main conclusions are as follows:

(1) A critical theoretical model for cavity maintenance is developed and verified. By integrating the structural dynamics of the drilling mechanism with the inverse effect of cylindrical cavity expansion, a critical theoretical model is successfully constructed. This model not only deduces the essential conditions for cavity stability and identifies the key influencing parameters, but also validates its accuracy through case analysis and demonstrates that soil cohesion is the dominant factor governing cavity collapse. This fundamental model provides a solid theoretical foundation for the subsequent optimization of operational parameters.

(2) Operational parameters are experimentally optimized and validated. A soil-bin experiment is conducted under the guidance of key parameters derived from the theoretical model. A predictive regression model is established using a quadratic orthogonal rotary central composite design. The optimal parameter combination is obtained via multi-objective optimization: mechanism operating frequency 34.9 r/min, soil moisture content 30%, drill bit rotational speed 173.2 r/min. A verification test is then carried out, and the measured results are highly consistent with the predicted values, with a maximum relative error of 10.3%. This result confirms the reliability of the proposed theoretical–experimental integrated method.

This work forms a closed loop between theoretical analysis and experimental validation, providing a feasible method and accurate operational guidance for cavity stability control in agricultural drilling machinery. Due to the limitations of experimental conditions and research period, only sandy loam soil from Shandong Province was tested in this study. Future research can extend mechanized drilling experiments to various soil types (e.g., black soil, red soil) in different regions, which will effectively expand the engineering application scope of the proposed drilling mechanism.

Acknowledgements

This research was supported by the Hainan Provincial Key Research and Development Program (Grant No. ZDYF2026XDNY146), Hunan Provincial Natural Science Foundation of China (Grant No. 2024JJ6227), and National Modern Agricultural Industry Technology System Post Scientist Project (Grant No. CARS-33-JX2).

[References]

[1] Qiu X B, Gao C W, Chen W, Liang G L, Tu Y G. Effects of soil temperature and humidity on early stage growth and development of tobacco plants by well-cellar transplanting. Tobacco Science &

Technology, 2015; 48(7): 20–24, 35. (in Chinese)

[2] Han C J, Ge P, Guo H, Zhan J, Zhang X J. Design and simulation analysis of multi-bar punch mechanism. Journal of Agricultural Mechanization Research, 2019; 41(10): 135–140. (in Chinese)

[3] Cheng Y D, Tan X B, Liu Q, Yang C C, Shi P Q, Jia M, et al. Effects of different seeding height on growth, yield and quality of tobacco under well-cellar transplanting. Shandong Agricultural Sciences, 2019; 51(11): 44–48.

[4] Yu L H, Xu Z B, Han Z L, Pan D B, Zhang F G. Adaptability analysis of mechanized transplanting of pepper in hilly mountainous area. Journal of Agricultural Mechanization Research, 2020; 42(10): 184–188, 194. (in Chinese)

[5] Zhou M L, Shan Y Y, Xue X L, Yin D Q. Theoretical analysis and development of a mechanism with punching device for transplanting potted vegetable seedlings. Int J Agric & Biol Eng, 2020; 13(4): 85–92.

[6] Shi J W, Li J, Liu W, Yue R C, Zhang T F, et al. Design and experiment of planting mechanism of automatic transplanter for densely planted vegetables. Agriculture, 2024; 14: 1357.

[7] Zhao S Y, Liu J Z, Jin Y C, Bai Z C, Liu J L, Zhou X. Design and testing of an intelligent multi-functional seedling transplanting system. Agronomy, 2022; 12(11): 2683–2683.

[8] Fan Y Y, Zhang X L, Li J H, Wang D. Design and test of tobacco cellar-type transplanter. Journal of Chinese Agricultural Mechanization, 2020; 41(5): 40–46. (in Chinese)

[9] Zhang D B, Zhang Y C, Zhang Y F, Li Z. Design and locomotion characteristics analysis of cavitation mechanism of intermittent mobile tobacco seedlings transplanter. Journal of Agricultural Mechanization Research, 2021; 43(3): 106–112. (in Chinese)

[10] Xu G W, Jian S C, Song Y M, Fang H M, Qiu X Y, Ming X L. Design and experiment of cellar cavitation mechanism for crops of hilly mountains transplanter. Transactions of the CSAM, 2022; 53(3): 105–113, 125. (in Chinese)

[11] Xu G W, Fang H M, Song Y M, Du W S. Optimal design and analysis of cavitating law for well-cellar cavitating mechanism based on MBD-DEM bidirectional coupling model. Agriculture, 2023; 13(1): 142.

[12] Li B, Tang M X, Hu H S, Liu C L, Ling Z, Su D L, et al. Theoretical analysis of drilling unloading and pile-side soil pressure recovery of nonsqueezing pipe piles installed in K0-consolidated soils. Buildings, 2024; 14(6): 1670. (in Chinese)

[13] Ding Y, Liu X J, Luo P Y. Investigation on influence of drilling unloading on wellbore stability in clay shale formation. Petroleum Science, 2020; 17(3): 1–16.

[14] Vesić A S. Expansion of cavities in infinite soil mass. Journal of the Soil Mechanics and Foundations Division, 1972; 98(3): 265–290.

[15] Zhang X L, Zhao J M, Du X L. Computation method for soil resistance around pile based on cavity expansion theory. China J. Highw. Transp., 2021; 34(6): 19–26.

[16] Haythem G, Mustafa J, Alain H. Pile end bearing capacity in rock mass using cavity expansion theory. Journal of Rock Mechanics and Geotechnical Engineering, 2020; 12(5): 1103–1111.

[17] Suman M, Noriyuki Y. Vertical bearing capacity of tapered piles in sands using cavity expansion theory. Soils and Foundations, 2013; 53(6): 853–867.

[18] Chen C F, Li W, Zhu S M, Chen Y L. Method for calculating soil-grout interface bond strength of pressure-grouted anchors based on viscoelastic-plastic cavity expansion theory. China J. Highw. Transp., 2022; 36(2): 41–51. (in Chinese)

[19] Li C, Mo P Q. Energy dissipation analysis for large-strain cylindrical cavity expansion problem in cohesive-frictional soils. Applied Mathematical Modelling, 2022; 111: 681–695.

[20] Joakim J, Jens K H, Thomas L W, Tore B. Cylindrical cavity expansion approximations using different constitutive models for the target material. International Journal of Protective Structures, 2018; 9(2): 199–225.

[21] Xu J, Dai G L, Gong W M. Elastoplastic analysis of normal stiffness of bore wall of the rock-socketed pile based on Hoek-Brown failure criterion and cavity expansion theory. Japanese Geotechnical Society Special Publication, 2020; 8(7): 239–244.

[22] Xiong G J, Wang J H, Chen J J. Stability analysis and support suggestions of pile hole stability analysis and support suggestions of pile hole based on mud pressure balance earth pressure. Journal of Shanghai Jiaotong University, 2021; 55(9): 1108–1115. (in Chinese)

[23] Chen S L, Abousleiman Y N. Exact undrained elasto-plastic solution for cylindrical cavity expansion in modified cam clay soil. Géotechnique, 2012; 62(5): 447–456.

[24] Zhang W M, Guo F W, Zhao Y. Elasto-plastic solution for undrained cylindrical cavity expansion in refuse soil. Scientific Reports, 2024; 14(1): 30126.

[25] Cao L J, Zhao J H, Wei X Y. Stress analysis of lime-soil compacted pile based on the unified strength theory. Rock and Soil Mechanics, 2026; 27(10): 1786. (in Chinese)

[26] Randolph M F. Science and empiricism in pile foundation design. Géotechnique, 2003; 53(10): 847–875.

[27] Zhou M R, Lu G W, Wang T, Wang J W. Mechanism analysis of structured loess fracturing grouting. Engineering Mechanics, 2019; 36(3): 169–181. (in Chinese)

[28] Li L, Li J P, Gong W B, Zhang L X. Elasto-plastic solution to expansion of a cylindrical cavity in K0-consolidated natural saturated clay. Journal of Harbin Institute of Technology, 2017; 49(6): 90–95. (in Chinese)

[29] Zheng J H, Qi C G, Wang X Q, Shan Y L, Lai W J, Wang L Z. Elasto-plastic analysis of cylindrical cavity expansion considering particle breakage of sand. Chinese Journal of Geotechnical Engineering, 2019; 41(11): 2156–2164. (in Chinese)

[30] Huang C L, Wang Z Q, Li S T, Chen Y Q, Dai M N, Wu W, et al. Coupling algorithm of cavity expansion theory and finite element for penetrating reinforced concrete. Engineering Fracture Mechanics, 2024; 110580. DOI: 10.1016/j.engfracmech.2024.110580

[31] Yu L L, Zhang F G, Liu G H, Qi Y M. Study on working mechanism and adaptability of well-cellar making for tobacco transplanting. Machinery Design & Manufacture, 2018; 4: 97–100.

[32] Hu C S, Yu L H, Xu Z B, Zhang F G, Chen Y. Improvement and experiment main component of well-cellar making machine for tobacco seedling transplanting. Journal of Agricultural Mechanization Research, 2019; 41(10): 198–202.

[33] Tang L, Yang X S, Zha X D, Zhou Y, Jiang L. Experiment on shear strength relation model of remolded low liquid limit clay based on water content. Journal of Changsha University of Science and Technology (Natural Science), 2021; 18(2): 26–32. (in Chinese)

[34] Meng C, Yang W, Bai Y, Li H, Zhang H, Li M Z. Research of soil surface image occlusion removal and inpainting based on GAN used for estimation of farmland soil moisture content. Computers and Electronics in Agriculture, 2023; 212: 108155.

[35] Alec M, Andrea F, Schalk W J. Assessment of the posttunneling safety factor of piles under drained soil conditions. Journal of Geotechnical and Geoenvironmental Engineering, 2020; 146(9): 0002348.

[36] Xu S, Zhang D B, Ma X W, Zhang Y F, Zhang Y J, Zhang Y C, et al. Study on the influence of drill bit structure on the quality of tobacco seedling transplantation. Journal of Agricultural Mechanization Research, 2021; 43(3): 182–188.

[37] Zohreh A, Riley E, Daniel S, Ahmed L, John L, Andrew W, et al. An efficient soil moisture sampling scheme for the improvement of remotely sensed soil moisture validation over an agricultural field. Geoderma, 2024; 442: 116763.

[38] Yang Q Z, Shi L, Shi A P, Hao M S, Zhao X Q, Zhang L, et al. Determination of key soil characteristic parameters using angle of repose and direct shear stress test. Int J Agric & Biol Eng, 2023; 16(3): 143–150.

[39] Ahmad F, Qiu B J, Ding Q S, Ding W M, Khan Z M, Shoaib M, et al. Discrete element method simulation of disc type furrow openers in paddy soil. Int J Agric & Biol Eng, 2020; 13(4): 103–110.

[40] Shen Y, Yang F, Wu J B, Luo S, Khan Z, Zhang L K, et al. Advances and future trends in electrified agricultural machinery for sustainable agriculture. Agriculture, 2025; 15(22): 2367.

[41] Zhao Z, Huang H D, Yin J J, Yang S X. Dynamic analysis and reliability design of round baler feeding device for rice straw harvest. Biosystems Engineering, 2018; 174: 10–19.

[42] Tang Z, Wang H Y, Tian L Q, Lao L Y, Sun H Y. Enhancing grain harvester fatigue reliability to support sustainable agriculture: A review of research status and prospects. Science Progress, 2025; 108(4): 368504251400813.

[43] Han D L, Ren L Z, Li C W, Liu H R, Hu J R, Yang D Y, Yang Q Z. Mechanical response of wet and soft soil to complex interactions with solid. Soil and Tillage Research, 2026; 255: 106834.

[44] Wu S, Wei X H. Mechanical interaction between a canopy opener and rice stalks based on the transient dynamic analysis. Biosystems Engineering, 2019; 178: 256–263.